Journal of Molecular Liquids 337 (2021) 116504

Contents lists available at ScienceDirect

Journal of Molecular Liquids

journal homepage: www.elsevier.com/locate/molliq

Molecular recognition of synthesized halogenated chalcone by calf thymus DNA through multispectroscopic studies and analysis the anti-cancer, anti-bacterial activity of the compounds

Abhijit Mukherjee [a,1,*], Suvranil Ghosh [b,1], Sudipta Ghosh [c], Sachinta Mahato [a], Mahadeb Pal [b,*], Sukanta Kumar Sen [c], Adinath Majee [a], Bula Singh [a,*]

[a] Department of Chemistry, Siksha-Bhavana, Visva-Bharati University, Santiniketan 731235, West Bengal, India
[b] Division of Molecular Medicine, Bose Institute, P-1/12 CIT Scheme VII-M, Kolkata 700054, West Bengal, India
[c] Department of Botany, Siksha-Bhavana, Visva-Bharati University, Santiniketan 731235, West Bengal, India

ARTICLE INFO

Article history:
Received 30 July 2020
Revised 17 April 2021
Accepted 14 May 2021
Available online 21 May 2021
This article is dedicated to the memory of wonderful researcher and flutist Abir Maji.

Keywords:
Calf thymus DNA
Chalcone
Cytotoxicity
Apoptosis
Spectroscopic study
Docking

ABSTRACT

The present study aims to elucidate the anti-cancer, antimicrobial activity of synthesized halogenated chalcones (1f, 1h, 1i) and their molecular interaction with calf thymus DNA. All the three compounds were characterized using different spectroscopic tools like FTIR, NMR. DFT and TDDFT computation were performed to support the structural and electronic parameter of the compounds. UV–vis absorbance, steady-state fluorescence, time-resolved fluorescence, circular dichroism, helix melting, molecular docking study reveals that the compounds (1f, 1h, 1i) actively interact with ctDNA via groove binding mode. The binding constants (K_b) were calculated to be 1.29×10^4, 0.54×10^4 and 0.45×10^4 M^{-1} respectively for compounds 1f, 1h, 1i. The compounds were cytotoxic to almost every cell line (PC3, HeLa, A549, HCT116) tested, having minimal toxicity in normal NKE cell line, among which PC3 cells were more sensitive with an IC_{50} value of 10 μM. The values were determined using dose response curve and found between 10 and 49 μM for cancer cells and 70 μM for normal cell. Compounds also cause apoptosis in PC3 cells, which was confirmed by Annexin V-FITC/PI assay. Results showed that 1f, 1h, 1i target DNA, to persuade DNA damage mediated cancer cell death. The inhibition zone was formed in the screening test indicating the anti-bacterial activity of 1f, 1h & 1i against model pathogenic bacteria. So the present communication provides quantitative insight of halo-chalcone based anti-cancerous and antimicrobial molecule involving relevant target nucleic acid, which holds future promise in the development of new therapeutic agents.

© 2021 Published by Elsevier B.V.

1. Introduction

Cancer, a global threat, claims about 9.56 million deaths and 18.1 million new cases during the past year [1a] creating a global burden on human beings and the world economy. Among various cancers, lung cancer, colon cancer, breast cancer, and prostate cancer killed huge percent of lives worldwide [1b]. Current therapeutic regimen for cancer relies on chemotherapy and radiation therapy, although both have severe toxic side effects on patients and increases the chance of recurrence of the disease. Moreover escalated cost of these treatments limits the scope for people who lived in lower economic conditions. Immense efforts are being made to develop specific, potent, and affordable cancer chemotherapeutics, but the finding of an explicit remedy is still a challenge. So there is a constant need to synthesize bioactive small molecules like chalcone one kind of flavonoids that can recognize the DNA, proteins, or other molecules in a cancer cell by target-specific manner and destroy them [2–7]. In this regard, we have synthesized three different halogen-substituted chalcones (1f, 1h, 1i) to find out a new type of therapeutic agent against cancer.

Flavonoids are the natural secondary metabolites having a polyphenolic structure, widely found in fruits, vegetables and certain beverages which were reported to be used as food for different ailments from ancient times. Flavonoids have various medicinal properties like antimicrobial, [8a,b] antioxidant,[8c] antiviral, antifungal, [8d] and anticancer,[8e] activities while

* Corresponding authors.
E-mail addresses: abhijitmukherjee.rs@visva-bharati.ac.in, abhijt.chem@gmail.com(A. Mukherjee), mahadeb@jcbose.ac.in (M. Pal), bulasingh@visva-bharati.ac.in (B. Singh).
[1] Equal contribution on the work.

https://doi.org/10.1016/j.molliq.2021.116504
0167-7322/© 2021 Published by Elsevier B.V.

having minimal toxicity in mammalian cells [8 f,g]. Chalcone, a unique class of flavonoids consists of two aromatic ring systems separated by a three carbon linker of an α,β-unsaturated carbonyl moiety in its structure. The presence of various groups on both the phenyl ring can exhibit a variety of pharmacological properties which arise due to the presence of double bonds in conjugation with carbonyl functionality [8h].

On the other hand DNA plays a major role in the life process because it carries heritage information and facilitates the biological synthesis of proteins and enzyme through replication and transcription of genetic information.[9] It is also been reported that the association of small molecule with nucleic acids acts as a controlling tool of the DNA functions in the diagnostic application, bioimaging, gene-delivery, therapeutic method and also for supervising the structural reorganization of biomacromolecule in the living cells.[10–12] DNA binding with the small molecules is crucially affected by different kind of binding forces.[13] Generally DNA binders are associated to the helical strand through two discrete manners: groove binding and intercalation.[14–17] For that reason such small molecule are assuring prospect for molecular recognition strategy in the field of biological science. [18–21]

However, to the best of our knowledge there has been no such report on the anti-cancer activity of synthesized halogenated chalcone molecules 1f, 1h, 1i and their molecular interaction with ctDNA till date. In our study, we made an attempt to synthesize some beneficial chalcones to see their efficacy against potent cancer cells, model bacteria and binding interaction with ctDNA which can be used as a targeted way to eradicate the future problems.

2. Experimental section

2.1. Materials

Doxorubicin, ctDNA sodium salt (CAS number: 73049395), Hoechst 33258, acridine orange (AO), urea were purchased from Sigma Aldrich, USA. 48well plate (Thermo scientific), MTT reagent, trypsin solution, penicillin and streptomycin, non essential amino acids and L-Glutamine were purchased from Himedia, India. FITC Annexin V apoptosis detection kit (Cat 556547) BD Pharmingen. Chalcone (1f) and its halogenated derivatives 1h, 1i used in the present study are shown in Scheme 1.

Details of synthesize, characterization by UV–vis, mass, ^{1}H and ^{13}C NMR spectral method are provided in the results and discussion. Ethidium bromide (EB) was purchased from Himedia, India. Tris-HCl buffer, Sodium chloride (NaCl), potassium iodide (KI) and other chemicals were purchased from SRL Pvt. limited, India. The antibody used in this study was purchased from Cell Signaling Technology (CST, USA) phospho-histone H2A.X (Ser139, #9718) and secondary anti-rabbit secondary antibody (ab6721) was purchased from Abcam. All the other chemicals were of reagent grade and needed no further purification. All the experiment was carried out using Milli-Q (Milli pore) water.

2.2. Cell line

PC3, A549, HCT116 (carrying functional p53 protein), HeLa and NKE were obtained from ATCC, USA. The cells were grown either in Dulbecco's modified Eagle's medium (DMEM; Gibco) or Roswell Park Memorial Institute (RPMI) 1640. Media were supplemented with 10% fetal bovine serum (Invitrogen), 0.1 mM nonessential amino acid, 1 mM L-Glutamine, 50 μg/ml penicillin, 50 μg/ml streptomycin and 2.5 μg/ml amphotericin B. Cells were maintained in a humidified environment at 37 °C with 5% CO_2.

2.3. Methods

2.3.1. Preparation of sample

The stock solution of 1f, 1h and 1i was prepared in minimum amount of DMSO while ctDNA was dissolved in 0.01 M Tris-HCl buffer at pH 7.4 and a homogenous solution was obtained with occasional mixing for 24 h. Determining the absorbance ratio A_{260}/A_{280} nm the purity of the ctDNA solution was checked. The concentrations of ctDNA solutions were determined by using the molar extinction coefficient value of 6600 M^{-1} cm^{-1} at 260 nm, which was found in the range of 1.8–1.9, indicating that ctDNA was free from protein.

2.3.2. Computational methodology

All theoretical calculations of compounds 1f, 1h and 1i were performed with the help of density functional theory (DFT) as implemented in Gaussian 09 [22] suite of programs. The calculations through out the present study were performed with B3LYP hybrid functional, [23] which includes Hartree-Fock (HF) exchange as well as DFT exchange correlations. The non-local correlations part is taken care by Lee, Yang and Parr (LYP) functional. All calculations were performed using Pople's 6-31G(d) basis set.

2.3.3. Biological activity

Cell cytotoxicity and antimicrobacterial activity of the compound was determined by using MTT assay, agar well-diffusion methods and details of the FITC-Annexin V/ PI assay, DAPI staining, estimation of minimum inhibitory concentration (MIC), minimum bactericidal concentration (MBC), hemolytic assay are provided in the supporting information (SI).

2.3.4. Molecular recognition of 1f, 1h and 1i by ctDNA

2.3.4.1. UV–visible spectroscopy. UV–vis spectroscopic measurement was performed using a Shimadzu dual beam UV–vis spectrophotometer (UV-1800, Japan) in 0.01 M Tris-buffer (pH 7.4). The compounds 1f, 1h, 1i were dissolved in minimum amount of DMSO at a concentration of 0.001(M). Working solutions were

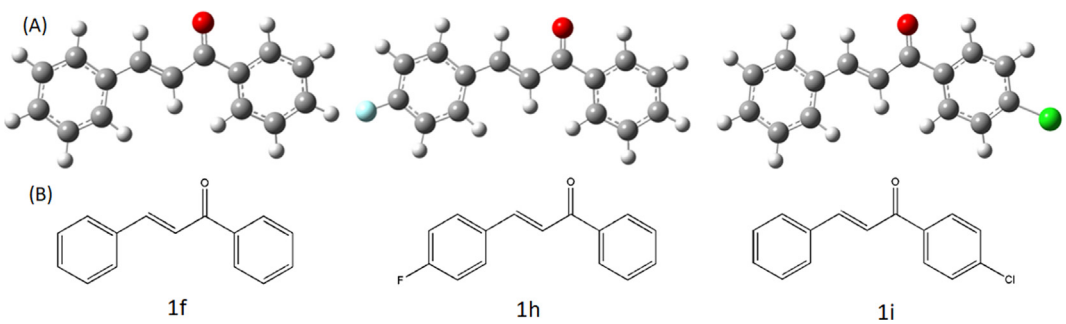

Scheme 1. (A) Optimized structures and (B) Chemical structures of 1f, 1 h and 1i.

prepared by dilution of the 1f, 1h, 1i in DMSO in 0.01 M Tris-buffer as required. The concentration of ctDNA (purchased from Sigma-Aldrich, USA) was varied from 0 to 60 μM. All measurements were taken at 298 K.[24]

2.3.4.2. Fluorescence studies.

2.3.4.2.1. Steady state and time resolved fluorescence measurement. Fluorescence experiments were carried out by fluorometric titration using a Hitachi F-7100 spectrophotometer equipped with a xenon flash lamp using 1.0 cm quartz cells. The excitation of 1f, 1h, 1i was done at 335 nm and the emission spectra were recorded in the range of 350–550 nm, with the widths of both the excitation and the emission slits 10 nm. The fluorescence titration was carried out by keeping the concentration of 1f, 1h, 1i constant at 10 μM in a reaction mixture of 2.5 ml and the ctDNA concentration was varied from 0 to 80 μM.

Time resolved fluorescence life time measurement was done using the time correlated single photon counting (TCSPC) technique.[25] After exciting the samples at λ_{ex} = 340 nm and using a picoseconds diode laser (IBH-NanoLED N-340 L light source with full width half maxima, fwhm, ~750 ps), the signals were collected at the magic angle polarization with the help of Hamamatsu MCP Photomultiplier (model R-3809U-50).[27] Goodness of fits was evaluated from the χ^2 criterion and visual observation of the residuals of the fitted functions to the data. The emission was fixed at 356 nm. For analyzing multiexponential fluorescence decay (I(t)) the following expression was employed.[25]

$$I(t) = \sum_i \alpha_i \exp(-t/\tau_i) \quad (1)$$

In which α_i stands for the pre-exponential factor (amplitude) regarding the i^{th} decay time constant τ_i.[25] The intensity of fluorescence of biexponential decay for a given λ is given by [26]

$$F_\lambda = \int_0^\infty F_\lambda(t)dt \quad (2)$$

Mean fluorescence lifetime (τ_{avg}) for exponential iterative fittings were calculated from the decay times (τ_1 and τ_2) and the normalized pre-exponential factors (a_1 and a_2) using the following relations.

$$\tau_{avg} = \tau_1 a_1 + \tau_2 a_2 \quad (3)$$

2.3.4.3. Competitive displacement assay. The ethidium bromide (EB) displacement assay was performed using 20 μM ctDNA in presence of 5 μM EB and titrated with an increasing concentration of 1f, 1h and 1i from 0 to 80 μM. The EB-ctDNA complex was excited at 475 nm and the emission spectra were recorded from 520 to 750 nm. Similarly AO-ctDNA complex was titrated with an increasing concentration of 1f, 1h and 1i from 0 to 80 μM upon excitation at 480 nm and the emission spectra were recorded between 500 and 670 nm. In the Hoechst 33,258 displacement assay, 5 μM Hoechst 33258, a well-known groove binder was added to 20 μM ctDNA and titrated with an increasing concentration of 1f, 1h, 1i from 0 to 80 μM. The Hoechst 33258-ctDNA complex was excited at 343 nm and the emission spectra were recorded from 400 to 650 nm.

2.3.4.4. Iodide quenching experiment. Iodide quenching studies were performed in the absence and presence of ctDNA. The emission spectra were recorded either in the absence or presence of 50 μM ctDNA in 3 ml of reaction mixture, which included 50 μM 1f, 1h and 1i and increasing concentrations of KI from 0 to 16 mM.

2.3.4.5. Effect of ionic strength. The effect of ionic strength was studied as reported earlier [27] by varying the concentration of NaCl between 0 and 50 mM in a total volume of 3 ml using 0.01 M Tris-HCl (pH 7.4) containing 1f, 1h, 1i and ctDNA (50 μM each) in two different experiments. Excitation was performed at 335 nm and the emission spectra were recorded from 350 to 550 nm.

2.3.4.6. DNA melting studies. The DNA melting study was performed in the absence and presence of 1f, 1h, 1i by monitoring the absorbance of ctDNA over a wide range of temperature ranging from 40° to 85 °C. The absorbance of the compounds were monitored at 260 nm and then plotted as a function of temperature. The values of the melting temperature (T_m) were determined as the transition midpoint of the melting curve.

2.3.4.7. Effect of urea. For further elucidate the binding interaction of 1f, 1h, 1i with ctDNA with the help of denaturation study, we have employed urea as a denaturataing agent. In a fixed volume of ctDNA bound 1f, 1h, 1i complex, in which both ctDNA and 1f, 1h, 1i are in same concentration, was titrated with varying the concentration of urea from 0 to 1(M). Upon exciting the complex at 335 nm the emission spectra were recorded from 350 to 550 nm.

2.3.4.8. Circular dichroism spectral studies. Circular dichroism measurements of ctDNA alone and 1f, 1h, 1i bounded ctDNA were recorded on a JASCO (J-815) spectropolarimeter which was connected with a highly sensitive temperature controller unit, applying a cylindrical cuvette of 0.1 cm path-length at 298 K. The described CD profiles were recorded in a range from 200 to 320 nm with a mean of four consecutive scans obtained at 20 nm min^{-1} scan rate with properly rectified baseline. The background spectrum of the buffer solution (0.01 M Tris-HCl, pH 7.4) was subtracted from the spectra of ctDNA and the 1f, 1h, 1i-ctDNA complex. The molar ratios of ctDNA concentration to 1f, 1h, and 1i concentration were 1:0, 1:0.5, 1:1 1:1.5, 1:2, 1:2.5 and 1:5. An average of four scans was taken in all the experiments.

2.3.4.9. Molecular modelling and docking. The molecular docking analysis for the binding interaction of 1f, 1h, 1i with ctDNA was carried out with Auto Dock 4.2 set of programs which utilizes the Lamarckian Genetic Algorithm (LGA) implemented therein. From the protein data bank the endemic 3D structure of B-DNA (for docking analysis) has consented bearing PDB ID: 1BNA.[28] The necessary file of the 1f, 1h, 1i, for docking with ctDNA, was produced through coupled usage of Gaussian 09 [22] and Auto Dock 4.2 [29] software packages. Appling Gaussian 09 suite of programs the geometry of 1f, 1h, 1i was first optimized at DFT/B3LYP/6-31G (d) level of theory. The resultant geometry of 1f, 1h, 1i was read in Auto Dock 4.2 software incompatible file format, from which the necessary file was created in Auto Dock 4.2. After adjusting the grid size to 60, 60, and 120 Å along X-, Y-, and Z-axis with a spacing of grid 0.375 Å. For the auto docking the following parameters are used. These are as follows: GA population size = 150; maximum number of energy evaluations = 2500000; GA crossover mode = two points. For each and every docking simulation the conformer which has lowest binding energy was searched out of ten different conformations, and for further analysis, consequent minimum energy structure was applied. The PyMOL software package was employed for visualizations of the docked conformation.[30]

3. Results and discussion

3.1. Synthesis and characterization

The chalcone and its halogen substituted derivative were synthesized using Claisen-Schmidt condensation reaction (Scheme 2) of substituted benzaldehyde (a) and different substituted

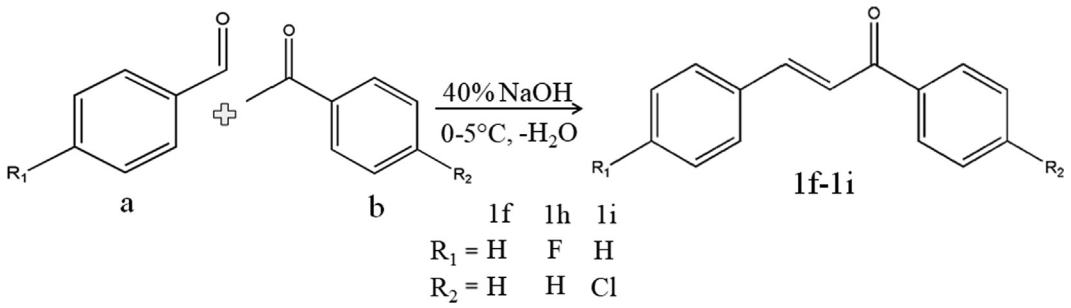

Scheme 2. General method of preparation of chalcone and its fluro and chloro substituted derivative.

acetophenones (b). The structures of the resulting chalcones (1f, 1h and 1i) were confirmed by UV, IR, mass,^{1}H and ^{13}C NMR spectral method.

(2E)-1,3-Diphenylprop-2-en-1-one (1f): Yield: 87% (304 mg); Pale yellow gummy mass; ^{1}H NMR ($CDCl_3$, 400 MHz): δ 8.17–8.14 (m, 2H), 7.96–7.88 (m, 3H), 7.75 (d, J = 6.4 Hz, 1H), 7.66–7.63 (m, 1H), 7.60–7.56 (m, 2H), 7.47–7.46 (m, 3H); ^{13}C NMR ($CDCl_3$, 100 MHz): δ 144.1, 139.9, 136.9, 131.7, 130.0, 129.9, 127.1, 126.6, 83.6, 45.9, 21.7, 21.3.

(E)-3-(4-fluorophenyl)-1-phenylprop-2-en-1-one (1h): Yield: 87% (304 mg); Pale yellow gummy mass; ^{1}H NMR ($CDCl_3$, 400 MHz): δ 8.17–8.14 (m, 2H), 8.00–7.89 (m, 3H), 7.75 (d, J = 6.4 Hz, 1H), 7.69–7.65 (m, 1H), 7.60–7.56 (m, 2H), 7.33–7.29 (m, 2H); ^{13}C NMR ($CDCl_3$, 100 MHz): δ 144.1, 139.9, 136.9, 131.7, 130.0, 129.9, 127.1, 126.6, 83.6, 45.9, 21.7, 21.3.

(E)-1-(4-chlorophenyl)-3-phenylprop-2-en-1-one (1i): Yield: 87% (304 mg); Pale yellow gummy mass; ^{1}H NMR ($CDCl_3$, 400 MHz): δ 8.20–8.17 (m, 2H), 7.96–7.89 (m, 3H), 7.76 (d, J = 6.4 Hz, 1H), 7.66–7.63 (m, 2H), 7.49–7.45 (m, 3H) ; ^{13}C NMR ($CDCl_3$, 100 MHz): δ 144.1, 139.9, 136.9, 131.7, 130.0, 129.9, 127.1, 126.6, 83.6, 45.9, 21.7, 21.3.

3.2. Biological study

3.2.1. Analysis of the cytotoxicity of the compounds

Cell proliferation assays were conducted with four different cancer cells (PC3, A549, HCT116 and HeLa) and normal NKE cells. Cell cytotoxicity of different compounds with a range of concentrations (0, 5, 10, 25, 50 μm) were assayed using MTT reagent, 3-(4, 5-dimethylthioazol-2-yl)-2,5-diphennyltetrazolium bromide as shown in Fig. 1. The number of surviving cell was disclose in terms of percentage of cell viability which is expressed as

$$\text{Percentage,(\%) of cellviability} = \frac{\text{Sample abs.@590nm(treatedcell)} - \text{background}}{\text{Control abs.@590nm(untreatedcell)} - \text{background}} \times 100$$

It was found that all compounds were highly cytotoxic towards PC3 cell line as compare to the other ones with the IC_{50} value of around 10 μm as shown in Table 1. IC_{50} of compounds in different cell lines is listed in the Table 1.

HCT116 cells were also sensitive like PC3 but IC_{50} value was higher for the compound 1i (25.07 ± 0.1173 μM). These compounds were less cytotoxic in HeLa and A549 cell lines. NKE cells were 7 fold less sensitive (IC_{50} around 70 μM) when compared to PC3 cell line (10 μM). From the results as shown in Fig. 1 it was clear that the compounds were cytotoxic and selective towards different cancer cell lines (highest in PC3) as compare to the normal NKE cell line. For further experimental set up we have chosen PC3 cell line.

3.2.2. Effect on cellular morphology

To assess the morphological change, PC3 cells were treated with two concentrations of the compounds (10 and 25 μM) for 24 h. Thereafter cellular morphologies were observed using an inverted phase contrast microscope (Leica phase contrast and fluorescence

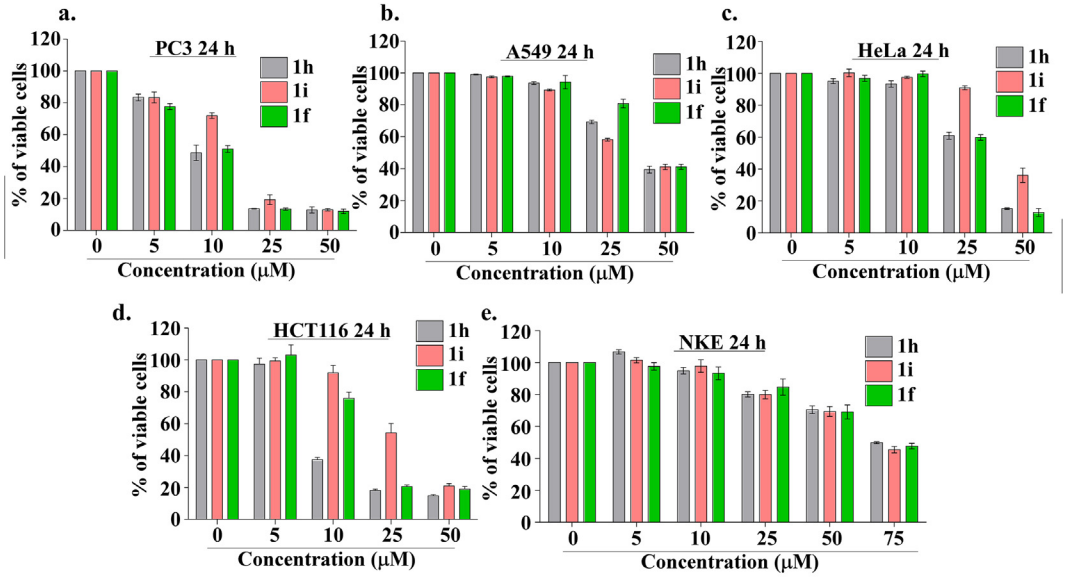

Fig. 1. Compounds are cytotoxic towards various cancer cell lines with minimal toxicity in normal cell line. The cell viability was measured by MTT assay using (a) PC3, (b) A549, (c) HeLa, (d) HCT116 cancer cell and (e) normal NKE cell lines with a range of concentrations (0–50 μM) of respective compounds (1h,1i,1f) for 24 h.

Table 1
IC_{50} values of the compounds 1f, 1h, 1i against different cancer cell line and normal NKE cell line.

Compound	PC3	A549	IC_{50} + SD(μM) HeLa	HCT116	NKE
1f	10.02 ± 0.13	25.63 ± 0.32	25.17 ± 0.07	10.50 ± 0.19	70.00 ± 0.15
1h	9.98 ± 0.12	25.35 ± 0.22	25.19 ± 0.09	9.779 ± 0.12	72.50 ± 0.50
1i	10.41 ± 0.17	49.85 ± 0.21	26.00 ± 0.52	25.07 ± 0.11	70.50 ± 0.41

microscope, at 40 × objective). Cells were shrinked, rounded, with disintegration of their membrane. Apoptotic vacuole like structure developed in the cells exposed to the compounds suggesting killing of the cell through apoptosis or autophagy in PC3 cells (Fig. 2).

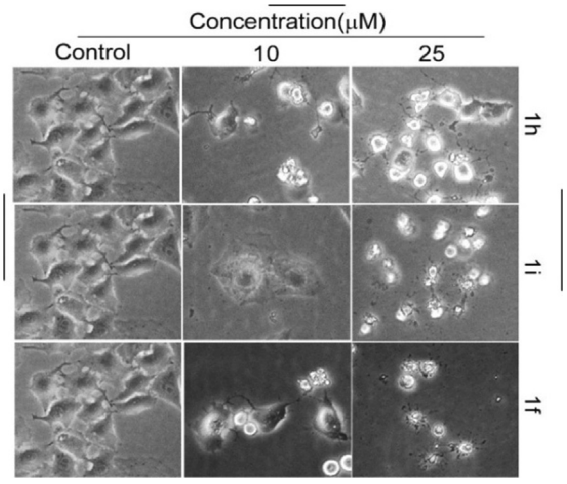

Fig. 2. PC3 cells were treated with two different concentrations (10, 25 μM) of the compounds 1h, 1i, 1f for 24 h. Images were captured using Leica phase contrast microscope (40X magnification).

3.2.3. 1f, 1h and 1i drive PC3 cells in the sub-G1 phase of the cell cycle

Next, the effects of the compounds on the cell cycle phases check points were tested. PI staining enables us to estimate the exact amount of DNA present in each phase of cell cycle. As shown treatment with the compounds led to the increase the population of PC3 cell in the sub-G1 phase of the cell cycle which is regarded as the apoptotic or necrotic cell population (Fig. 3). Treatment with 5, 10, and 25 μM of compounds led to an increase in sub-G1 phase in ascending manner from (1.39 to 38.56%), (1.58 to 24.81%), (1.78 to 29.40%), for 1h, 1i and 1f respectively as shown in Fig. 3.

3.2.4. 1f, 1h and 1i drives apoptotic death in PC3 cells

FITC-Annexin V/PI staining of PC3 cells were carried out to understand the mechanism of death of cells in response to treatment with these compounds. In this assay if death occurs by apoptosis, externalization of phosphatidyl serine occurs which will be otherwise present in the inner membrane.

Annexin V selectively binds with phosphatidyl serine resulting in FITC fluorescence indicating early apoptosis. In late apoptosis cell membrane including nuclear membrane and nuclei were fragmented. PI will gradually bind to the fragmented nuclei to signal late apoptosis. As shown in Fig. 4, treatment with these compounds for 24h with 10- and 25 μM resulted in dose dependent increase of apoptotic cells similar to doxorubicin (5 μM) was used as a positive control. This phenomenon was further confirmed by DAPI (4′,6-diamidino-2-phenylindole) staining which showed fragmented nuclei with increasing doses of the compounds like doxorubicin.

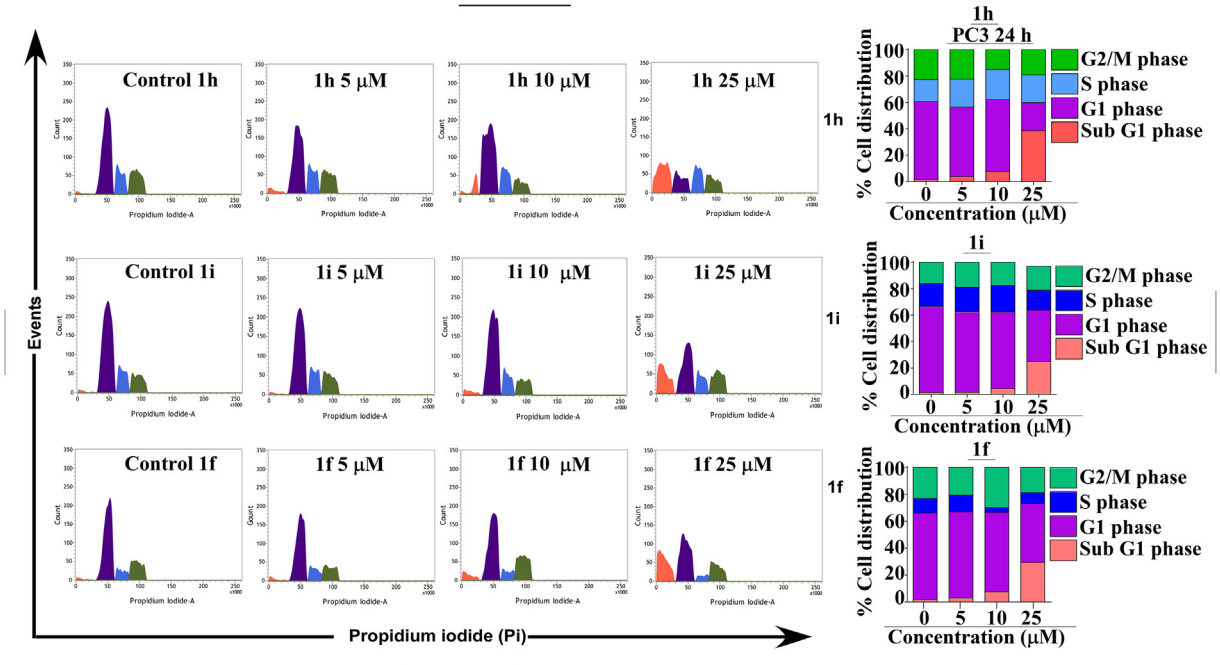

Fig. 3. Compounds increases sub-G1 population in PC3 cells upon treatment. (A) PC3 cells were treated with increasing concentrations (5–25 μM) of 1h, 1i, 1f for 24 h. DNA amount in different cell cycle phases were estimated by FACS (Propidium iodide PI staining) (1h, 1i, and 1f respectively). (B) Bar diagram are representative of distribution of cells in different cell cycle phases after treatment with various concentrations (5–25 μM) of 1h, 1i, and 1f respectively.

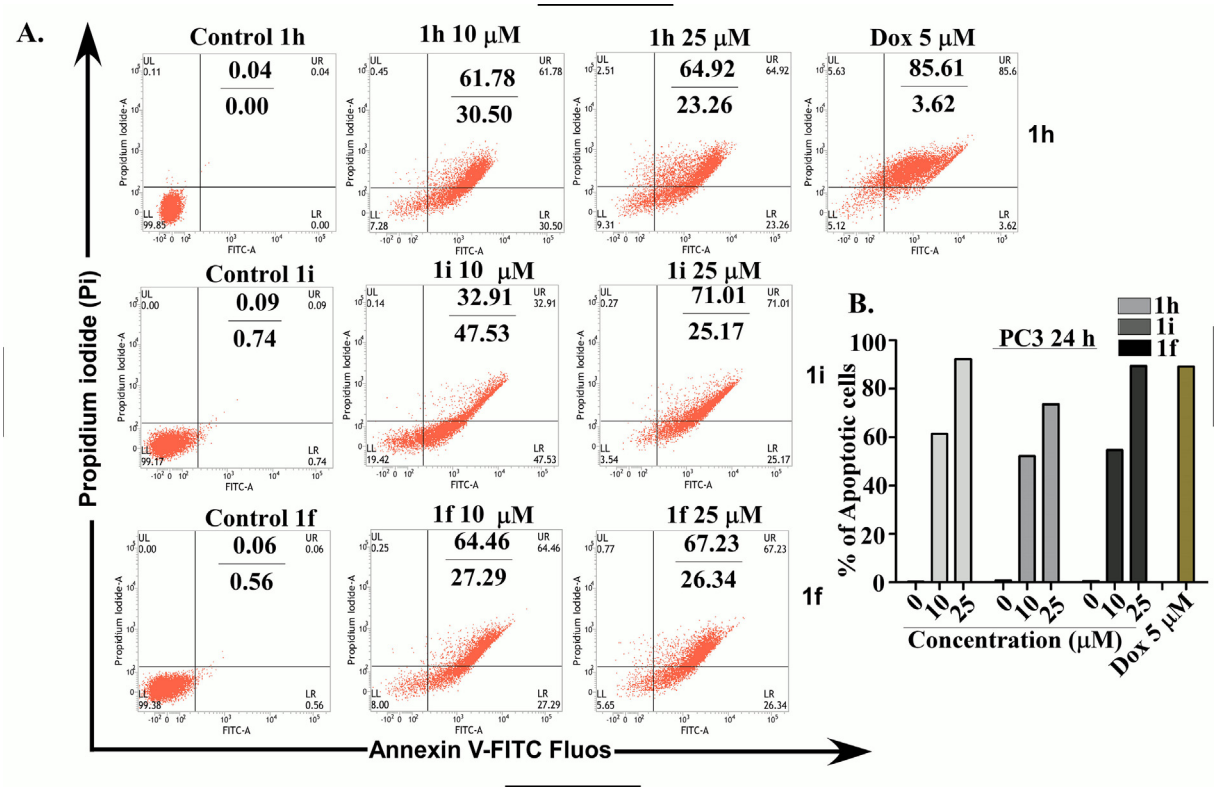

Fig. 4. Compounds induces apoptosis in PC3 cells in a dose dependent manner (A) PC3 cells were treated with 10 and 25 μM of 1h 1i and 1f for 24 h. Percentage of cells going to apoptosis (1h, 1i, and 1f respectively) was measured by staining the cells with AnnexinV-FITC/PI staining using FACS. (B) Bar diagrams is showing the percentage of apoptotic cells after treatment with 1h, 1i, and 1f respectively. Doxorubicin 5 μM was used as a positive control for apoptosis.

Here, PC3 cells were treated with two different doses of compound 1h, 1i, 1f (10 and 25 μM) for 24 h to stain with DAPI to visualize the effect on the cellular nuclei. As shown shrinked, condensed, and fragmented nuclei were resulted in cells exposed to the compounds compare to the mock treated control counterpart where nuclei appeared round in shape as shown in Fig. 5.

3.2.5. 1h, 1i and 1f targets DNA and induces DNA damage in PC3 cells

Several reports have shown that DNA damage can induce cell death by apoptosis.[31] To investigate the proper mechanism of death, PC3 cells were treated with two different concentrations (10 and 25 μM) of each of 1h, 1i, and 1f for 24 h to assess their effect on the phosphorylation of histone 2A.X (γ*H*2a.X) as the marker of DNA damage.[32] Phosphorylation at the ser139 of γH2a.X occurs in response to double strand break formation. Doxorubicin, a known anticancer drug which damages DNA by targeting DNA topoisomerase II was used as a positive control in the experiment. Immunoblot was then carried out using the whole cell extracts prepared from these cells. As shown in Fig. 6, treatments with 1f, 1h, 1i induced 4-fold increase in (γH2a.X) in compared to doxorubicin, which induces nine fold increases in the phosphorylation of (γH2a.X) in response to DNA damage.

3.2.6. In vitro antibacterial activity and hemolytic assay

In vitro antimicrobial screening of the purified compounds (1f, 1h & 1i) were investigated against pathogenic test bacteria of gram positive (*Bacillus subtilis* and *Staphylococcus aureus*) and gram negative (*Escherichia coli* and *Pseudomonas aeruginosa*) using the agar well-diffusion method.[33] The inhibition zone was formed in the screening test indicating the anti-bacterial activity of the tested compounds against Gram-negative bacteria (*E. coli* and *P. aeruginosa*) and Gram-positive bacteria (*B. subtilis*). But among those

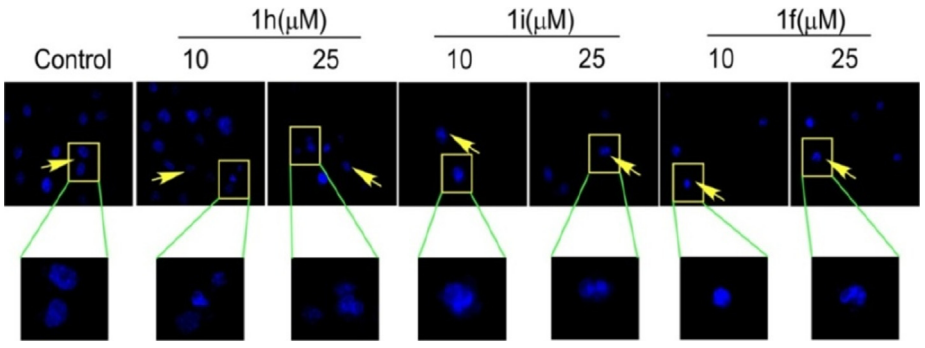

Fig. 5. Compounds induces nuclear fragmentation in PC3 cells. DAPI staining of 1h, 1i and 1f with two different concentrations (10, 25 μM) in PC3 cells for 24 h. Images were captured by inverted Leica fluorescence microscope with 40X magnification. Arrow heads represent the condensed and fragmented nuclei.

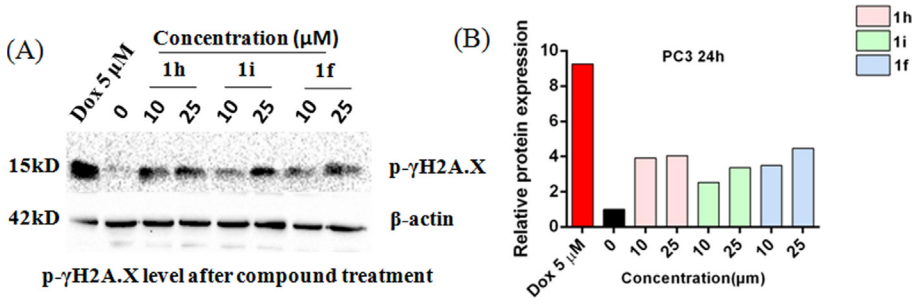

Fig. 6. Compounds potentiates DNA damage in PC3 cells upon treatment. (A) Representative immunoblot showing the upregulation of phospho- γH2a.Xlevel in PC3 cells after treatments with doxorubicin (Dox), 1h, 1i or 1f at the indicated concentrations for 24 h. β-actin was used as a loading control. (B) Bar graph showing the estimation of p-γH2a.X obtained by densitometric scanning of the immunoblots using Image J tool.

compounds (1f, 1i & 1h) no one is active against the gram positive bacteria *S. aureus*. The compound 1f produced relatively large inhibition zone against model pathogenic bacteria. The micro-dilution technique was used to determine MIC value of the tested compounds as shown in Table S3.

To determine the biocompatibility of the chalcone (1f) and its chloro and bromo substituted derivatives (1h, 1i) hemolytic assay is an important screening test. A large value of hemolysis leads to robust damage of the red blood cells and the compatibility of the 1f, 1h and 1i towards blood diminishes. Interestingly the compounds 1f, 1h and 1i exhibit a minor amount of hemolysis at the MIC for *B. subtilis, E.coli* and *P. aeruginosa*, respectively. The results of the dose dependent hemolysis of 1f, 1h and 1i are summarized in Table S4. From the results it can be said that the compounds are very effective for the bacteria *B. subtilis, E.coli* and *P. aeruginosa* and the effectiveness increases with increasing the concentration of 1f, 1h and 1i as shown in Table S4.Generally chalcone and its chloro and bromo substituted derivative displayed very good anti-hemolytic activity. Fig.S3 demonstrates a dose response profile of hemolysis of red blood cells in presence of 1f, 1h and 1i.

3.3. Molecular recognition of 1f, 1h and 1i by ctDNA

3.3.1. UV–vis absorption and emission study

The conventional biophysical techniques are applied to explore the interaction of bio-active 1f, 1h, 1i with ctDNA. To depict the structural changes and complex formation between the exogenous compounds (1f, 1h, 1i) with duplex ctDNA the UV–vis absorption spectroscopy was used.[24,34,35] In order to evaluate the mode of binding of the compounds 1f, 1h, 1i with ctDNA, absorption spectral titration were performed by adjusting a fixed concentration of the compounds at 20 μM and changing the ctDNA concentration from 0 to 50 μM. All the compounds shows an intense bands at 313–319 nm range and with gradual addition of ctDNA a decrease in the absorption intensity i.e. hypochromism was observed (1f = 19%, 1h = 15%, 1i = 13%) without any shift of the absorption maximum band (λ_{max}), which clearly indicate the complex formation between the 1f, 1h, 1i and ctDNA as shown in Fig. 7(a-c). To further illustrate the binding strength of the 1f, 1h, 1i with ctDNA, the binding constant (K_b) were calculated using the following equation:

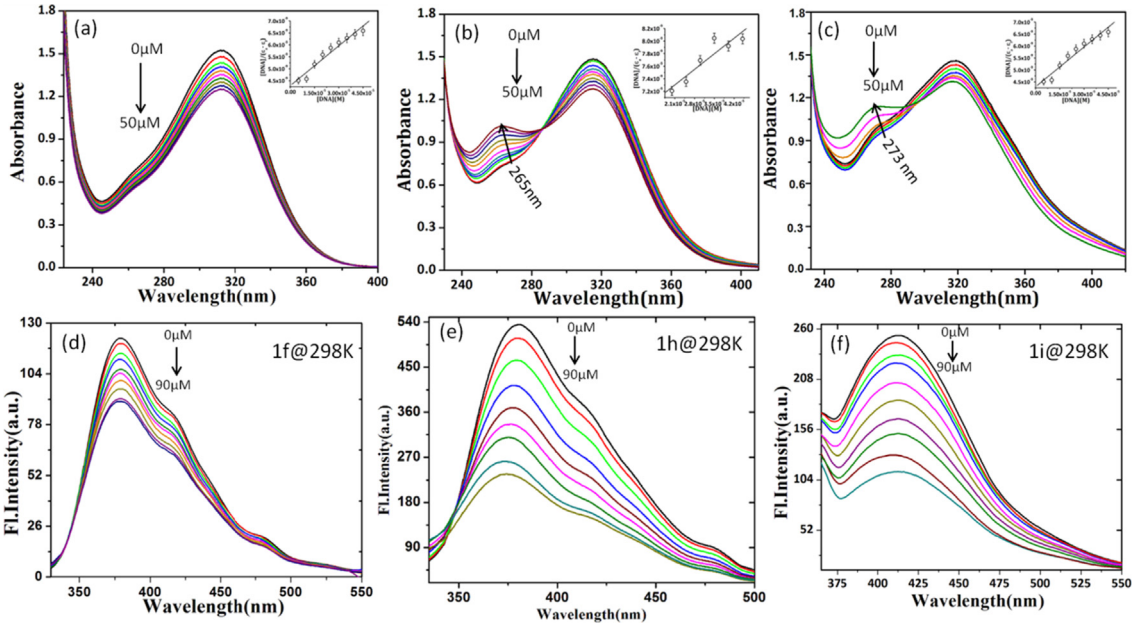

Fig. 7. (a-c) UV–vis absorption spectra of 1f, 1h, 1i (10 μM) with increasing concentration 0.0, 5, 10, 15, 20, 25, 30, 35,40,45 and 50 μM of ctDNA at pH 7.4 in 0.01 M Tris-HCl buffer (298 K). Inset: Plot of DNA/(ε_a- ε_f) vs.DNA for 1f, 1h, 1i-ctDNA system.(e-f) Fluorescence emission spectra of 1f, 1h, 1i (10 μM) in presence of 0–90 μM of ctDNA at 298 K (pH 7.4).

Table 2
Binding and thermodynamic parameters for the interaction of 1f, 1h and 1i with ctDNA.

Ligands	T(K)	K_f (L mol^{-1})	n	ΔH (kJ mol^{-1})	ΔS (J K^{-1} mol^{-1})	ΔG (kJ mol^{-1})
	288	0.162×10^4	1.1			−17.958
1f	298	0.257×10^4	1.3	33.167	177.52	−19.733
	308	0.389×10^4	1.2			−21.508
	288	1.09×10^4	1.4			−22.258
1h	298	1.22×10^4	1.2	9.392	109.90	−23.357
	308	1.42×10^4	1.1			−24.456
	288	0.917×10^4	1.3			−23.784
1i	298	0.970×10^4	1.4	6.822	99.37	−22.790
	308	1.12×10^4	1.2			−21.796

$$[DNA]/(\varepsilon_a - \varepsilon_f) = [DNA]/(\varepsilon_b - \varepsilon_f) + 1/K_b(\varepsilon_b - \varepsilon_f) \quad (4)$$

where [DNA] implies the concentration of ctDNA, ε_a is the excitation coefficient observed for 1f, 1 h, 1i of the absorption band at a given DNA concentration, ε_f is the excitation coefficient of free 1f, 1h, 1i and ε_b correspond to the excitation coefficient of 1f, 1h, 1i when fully bound to the ctDNA. The plots of DNA/ (ε_a- ε_f) as a function DNA gives a intercept 1/ K_b (ε_a- ε_f) and slope 1/ (ε_a- ε_f), the ratio of slope to intercept gives the intrinsic binding constant (K_b) value as shown in inset of Fig. 7 (a-c) and the values are tabulated in Table 2.It is found that the value of K_b is in the order of ~ 10^4 M^{-1} similar to those reported for classical non intercalating molecule [35].

To monitor the binding kinetics of 1f, 1h, 1i with ctDNA fluorescence spectroscopy was a well known tool. In Tris-HCl buffer solution 1f, 1h, 1i shows an unstructured emission spectrum with a peak around 379 nm, 381 nm, 412 nm upon excitation at 315 nm and both 1h, 1i at 320 nm. The gradual addition of ctDNA to the buffered solution of 1f, 1h, 1i leads to an appreciable decrease in the emission intensity without any shift of the emission maximum as shown in Fig. 7(d-f) and Fig. 8 .The fluorescence titration data are analyzed using the Stern-Volmer equation [25] to determine the Stern Volmer quenching constant (K_{SV}).

$$\frac{F_0}{F} = 1 + k_q.\tau_0[Q] = 1 + K_{SV}[Q] \quad (5)$$

where F_0 and F denote the fluorescence intensities in absence and presence of the quencher, respectively. The term k_q represents the quenching rate constant of biomolecule; τ_0 is the average lifetime of the biomolecule in absence of quencher and its value is 1.81 ns. K_{sv} is the Stern-Volmer quenching constant and [Q] stand for ctDNA concentration. The value of K_{sv} and k_q are listed in Table S6. The calculated binding constant value (normal range of binding constant for non-intercalating ~ 10^3–10^4 M^{-1}) [35] indicates the groove binding nature of the 1f,1h,1i in the ctDNA environment whereas for intercalative binding, the binding constants are known to be much higher (~10^5 M^{-1}). The data presented in Table S6 also reveal the linear relationship between the quenching effect of 1f, 1h, 1i with ctDNA, indicates a confirm formation of a ground state complex between the 1f, 1h, 1i and ctDNA. A static nature of quenching mechanism is also concluded as the calculated value of k_q is greater than that of the maximum scattering collision

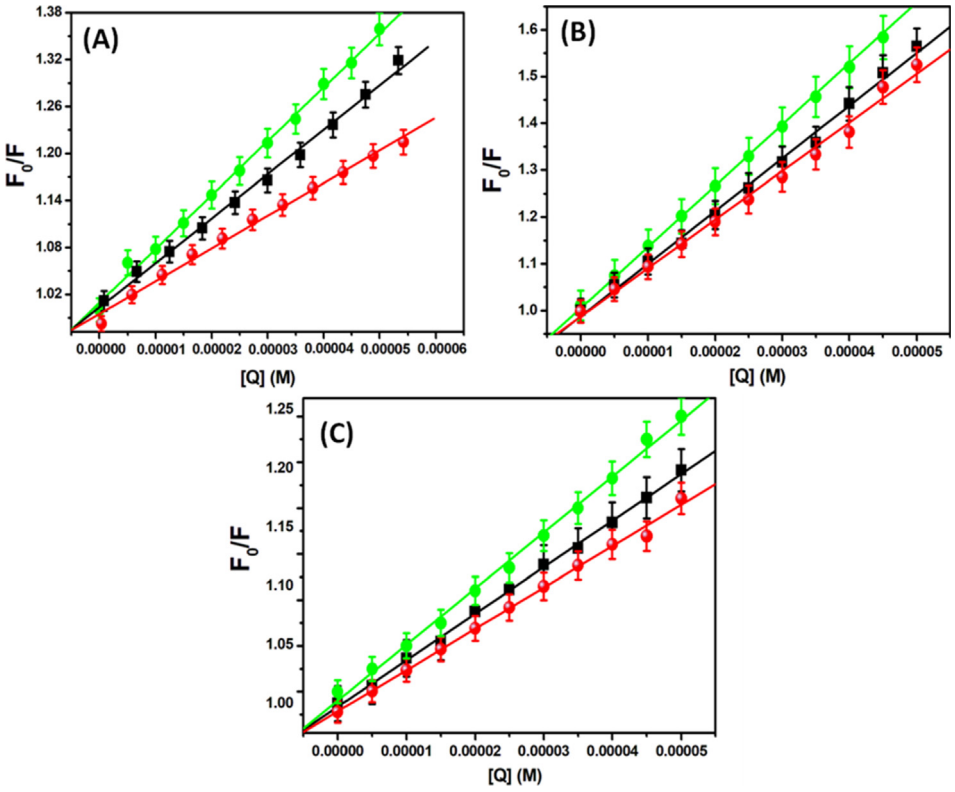

Fig. 8. The quenching effect graphs of 1f (A), 1h (B) 1i (C) at three temperatures (288, 298 and 308 K) obtained from the Stern–Volmer equation.

Table 3
Time-resolved fluorescence decay components of 1f, 1h, 1i in 0.01 M Tris-HCl buffer.

Compound	τ_1(ns)	τ_2(ns)	τ_3(ns)	α_1 (%)	α_2 (%)	α_3 (%)	τ_{avg}(ns)	χ^2
1f	1.02	5.38	0.11	23.04	23.78	53.18	1.57	1.04
1h	0.51	0.13	4.29	21.17	70.89	7.93	0.54	1.06
1i	0.15	11.9	0.23	10.98	26.38	62.64	3.32	1.08

Table 4
Calculation of the density functional reactivity descriptors of the base pairs of DNA and substituted chalcone compounds.

Compound	E_{HOMO} (a.u.)	E_{LUMO} (a.u.)	Chemical Potential (μ)	Chemical hardness (η)	Electrophilicity index (ω)
1f	−0.23235	−0.07738	−0.1548	0.0770	0.1550
1h	−0.23199	−0.07906	−0.1555	0.0764	0.1582
1i	−0.23668	−0.08370	−0.1601	0.0765	0.1675
Adenine	−0.21779	−0.01745	−0.1176	0.1002	0.0690
Guanine	−0.20808	−0.00591	−0.1069	0.1010	0.0565
Cytosine	−0.22684	−0.03065	−0.1287	0.0980	0.0845
Thymine	−0.24142	−0.03773	−0.1395	0.1018	0.0955

quenching constant. The static quenching nature of the present experiment is confirmed due to the obtained higher value of k_q as compared to the maximum diffusion scattering collision quenching rate of various quenchers with ctDNA ~ 2.0×10^{10} M^{-1} s^{-1}.[35] The detailed analysis of static and dynamics quenching is discussed in the next subsection using time-resolved fluorescence (TRF) technique.

3.3.2. Time-resolved fluorescence study

To analysis the exact nature of quenching, the fluorescence lifetime measurement was performed at a fixed concentration of 1f, 1h, 1i (20 μM) with varying concentration of ctDNA from 0 to 90 μM. The uncomplexed 1f, 1h and 1i was found to exhibit a tri-exponenetial decay pattern which comprises of major contribution from an ultrafast component and a minor contribution for slow components as shown in Table 4. It is observed that the fluorescence decay function remain unchanged with subsequent addition of ctDNA which reveals that the 1f, 1h, 1i-ctDNA interaction is driven by static quenching complex formation.[25] More detailed information is provided by calculating the biomolecular quenching rate constant k_q:[25]

$$k_q = \frac{K_{SV}}{\tau_0} \tag{6}$$

where K_{SV} is the stern-Volmer quenching constant and τ_0 is the lifetime of the 1f, 1h, and 1i in absence of ctDNA. The calculated value of k_q is summarised in Table 3. The present result indicates that a combination of specific short and long-range interaction between the 1f, 1h, 1i and ctDNA binding sites regulate the binding pathway as discussed in the next subsection.The static quenching nature can be further described by the following equation using the fluorescence intensity and concentration of the quencher.

$$\log\left[(F_0 - F)/F\right] = \log K_f + n\log[Q] \tag{7}$$

where K_f and n are the binding constant and the number of binding sites, respectively. From the plot of log[(F_0-F)/F] vs.log [Q] the binding constant (K_f) and the number of binding sites (n) can be determined as shown in Table 3.

The value of K_f was found in the range of $10^3 \sim 10^4$ M^{-1} at different temperature, which was nearly parallel to the binding constant (K_b) value, obtained from UV–vis absorbance results.

3.3.3. Elucidation of the thermodynamics parameters

To characterize the binding forces involved in the interaction of 1f, 1h and 1i with ctDNA, the relevant quenching data obtained from the steady state emission studies at different temperatures were analyzed according to the van't Hoff equation.

$$\log K_a = \frac{-\Delta H}{2.303RT} + \frac{\Delta S}{2.303R} = \frac{-\Delta G}{2.303RT} \tag{8}$$

where ΔH and ΔS are the changes in enthalpy and entropy respectively. According to Ross et al. the nature of interactive forces has been briefly summarized as: (a) ΔH < 0 and ΔS < 0 correspond to hydrogen bond formation, van der Waals interaction (b) ΔH > 0 and ΔS > 0 correspond to hydrophobic effect (c) ΔH < 0 and ΔS > 0 correspond to ionic/electrostatic interactions [34(b)]. The free energy change (ΔG) was determined using the equation.

$$\Delta G = \Delta H - T\Delta S \tag{9}$$

By plotting log K_a vs. reciprocal of absolute temperature (1/T) as shown in Fig. 9 we get the value of ΔH and ΔS from the slope and the intercept. The negative values of ΔG definitely apprise the feasibility of the process. Both the positive sign of ΔH and ΔS and their magnitudes are the hallmarks of hydrophobic interaction which is the driving force in binding interaction [34(c)]. The positive value of ΔH suggests that the interaction was endothermic in nature, which could be a good interpretation for the increased binding constant with the increase of temperature. Further analysis of the free energy contributions reveal that hydrophobic force of attraction also plays an important role in complex formation between 1f, 1h and 1i with ctDNA.

3.3.4. Comparative displacement assay

Comparative displacement assay with known DNA intercalators play an important role to decrypt the binding interaction of small molecule with DNA.[25,35–39] The most sensible fluorescent dye, planar acridine orange (AO), which binds with ctDNA through intercalative mode and appears as a weak fluorescent dye in Tris-HCl buffer solution, whereas, its fluorescence intensity is dramatically increased in close vicinity of ctDNA due to its intercalation within the ctDNA base pairs. [40,41]

This feature of AO is undertaken in several ctDNA binding studies to find out the binding fashion of new molecules with ctDNA. [36,37] Therefore, we choose AO-ctDNA interaction for competitor deracination experiment with 1f, 1h, 1i to find the nature of 1f, 1h, 1i-ctDNA interaction. It is found that there is no substantial alteration of fluorescence intensity of AO-ctDNA complex was observed with the subsequent increase of 1f, 1h, 1i concentration in the solution. It primarily indicates a non-intercalative type of binding between 1f, 1h, 1i and ctDNA.

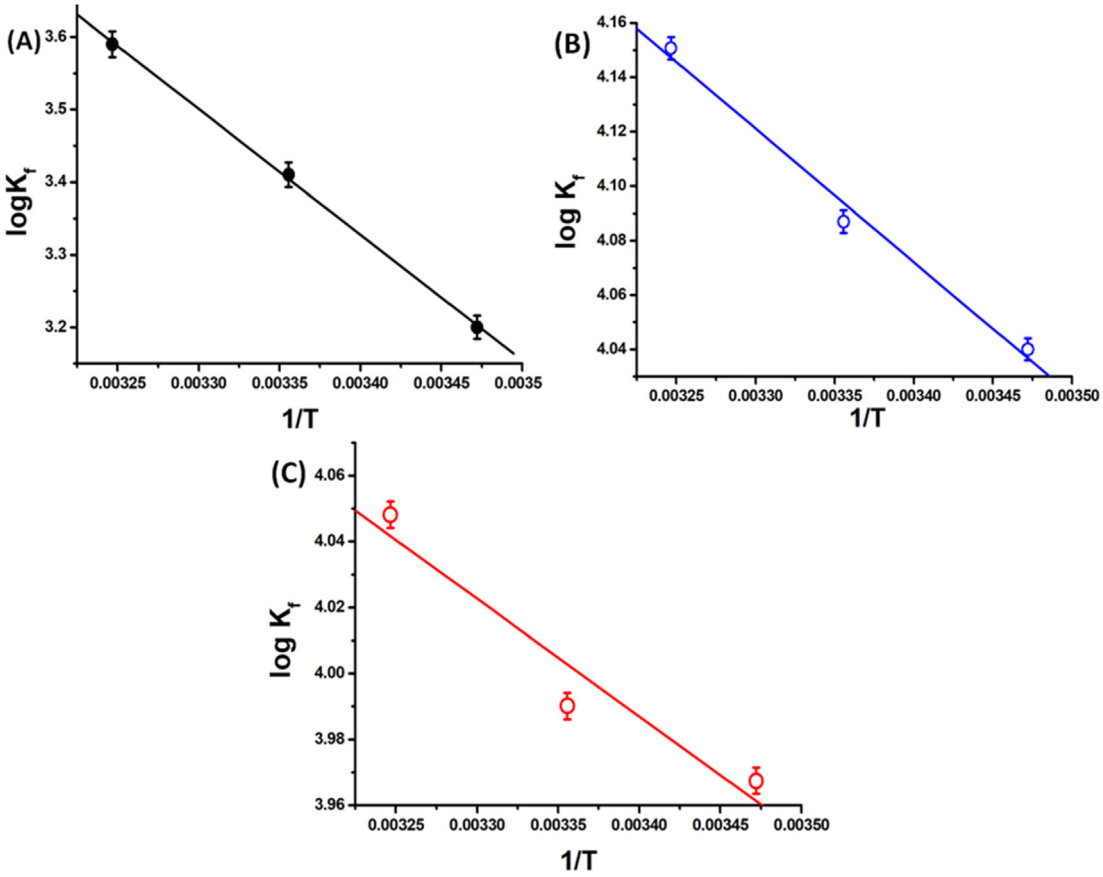

Fig. 9. Van't Hoff plot of the binding between 1f, 1h, 1i and ctDNA at 298, 304 and 310 K.

Further clarification of the binding interaction of 1f, 1h, 1i with ctDNA is performed with ethidium bromide (EB) replacement test considering the fact that EB is a sensible fluorescent dye which bears a planar structure and binds with ctDNA through intercalative mode.[38] It is found that the intensity of fluorescence of EB-ctDNA complex is unusually higher compare to its free form. We did not observe any noticeable change in the fluorescence intensity of EB-ctDNA complex on the subsequent variation of 1f, 1h, 1i concentration in the solution as shown in Fig. 8 (a-c). The present observation reveals that 1f, 1h, 1i is unable to exchange EB-ctDNA binding in the solution. Therefore, the present experiment also indicates a non-intercalative binding interaction of 1f, 1h, 1i with ctDNA as found in the previous experiment with EB-ctDNA complex. The results of the aforementioned experiments provide us a speculation of a possible minor groove binding between 1f, 1h, 1i and ctDNA. We have performed another dye replacement experiment with well-known minor groove binder Hoechst 33,258 which binds on to minor groove of the double helical ctDNA, to accomplish our speculation.[39] It is observed that a weak fluorescence of Hoechst 33,258 in Tris-HCl buffer medium is drastically increased in presence of ctDNA as shown in Fig. 10(d-f). This observation was attributed due to the minor groove binding of Hoechst 33,258 in the ctDNA helix. [42] In the present dye exchange experiment we found a noticeable quenching of fluorescence of Hoechst-ctDNA complex upon increase concentration of 1f, 1h, 1i. This indicates that 1f, 1h, 1i replaces Hoechst33258 from the minor groove of ctDNA. The result also suggests a groove binding between 1f, 1h, 1i and ctDNA through weak non-covalent interaction. The K_{sv} values for the quenching of EB, AO and Hoechst 33,258 bound to ctDNA by 1f, 1h, 1i was calculated using Stern-Volmer equation (2). The results are shown in Fig.S3 (a-c) and the values of K_{sv} are given in Table S1. The data given in Table.S1 reveals that the K_{sv} of Hoechst 33,258 is much higher as compared to the same of the EB and AO. Hence it can be concluded that 1f, 1h, 1i binds on the minor groove of ctDNA after displacing Hoechst 33258.

The binding interaction between 1f, 1h, 1i and ctDNA is again studied by fluorescence quenching experiment of 1f, 1h, 1i in presence and absence of ctDNA with well studied anionic quencher, potassium iodide (KI).[43,44] The results of this experiment is shown in Fig.S3 (d-f). The availability of small molecule to anionic quenchers (iodide ion) in presence of ctDNA and in free medium is studied using Stern-Volmer equation (2). The calculated K_{sv} value of free 1f, 1h, 1i by the iodide ions and the same in presence of ctDNA is summarized in Table S2. The similar value of K_{sv} obtained from fluorescence quenching experiments of 1f, 1h, 1i in presence and absence of ctDNA also ruled out the chance of intercalation between the 1f, 1h, 1i and ctDNA base pairs.

3.3.5. Effect of ionic strength

The effect of ionic strength is an efficient method to distinguish the binding interaction between 1f, 1h, 1i and ctDNA by performing a titration of 1f, 1h, 1i-ctDNA complex with NaCl. When NaCl is present in the system, then with increasing concentration of Na^+, the electrostatic repulsion between the negatively charged phosphate backbones on adjacent nucleotides is reduced. Thus, electrostatic interactions are shielded in the presence of Na^+ ions and the DNA chains will be tightened. Increased ionic strength screens the negatively charged phosphate backbone of DNA and weakens the interaction between ctDNA and 1f, 1h, 1i due to competition for phosphates. From this study we have found that after subsequent addition of NaCl (0–10.5 mM) into the 1f, 1h, 1i-ctDNA solution,

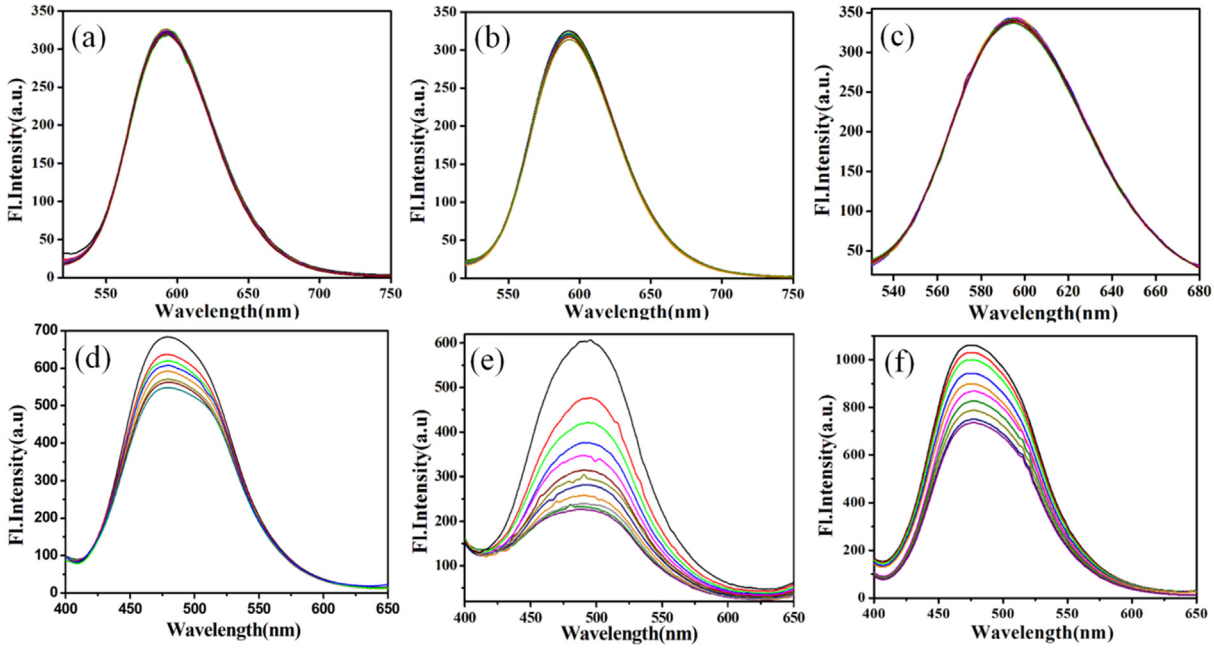

Fig.10. (a-c) Fluorescence emission spectra of EB bound ctDNA complex by increasing addition of 1f, 1h, 1i. In each titration concentration of ctDNA and dyes was fixed and variation of 1f, 1h, 1i was 0–100 μM; ctDNA = 20 μM. (d-f) Fluorescence emission spectra of Hoechst 33,258 bound ctDNA complex by increasing addition of 1f, 1h, 1i. In each titration concentration of ctDNA and dyes was fixed and variation of 1f, 1h, 1i was 0–100 μM; [ctDNA] = 20 μM in 0.01 M Tris-HCl buffer at pH 7.4.

no significant change in fluorescence intensity is observed as shown in Fig.S4 (d-f) in the SI, indicating that the electrostatic interaction may have a negligible role in the 1f, 1h, 1i-ctDNA interaction.

3.3.6. Denaturatating effect

The denaturatating effect of urea is utilized in conjunction with fluorescence technique to find out the binding nature of 1f, 1h, 1i-ctDNA complex.[24,43] The result of this experiment is presented in Fig.S4(a-c) and it indicates that there is no change of fluorescence intensity of the 1f, 1h, 1i-ctDNA complex (in buffer solution) after successive addition of urea. Hence, the result of the present experiment also indicates a non-intercalative type of binding interaction persists in between 1f, 1h, 1i and ctDNA in the 1f, 1h, 1i-ctDNA complex.

3.3.7. Study the conformational change of the ctDNA

The thermal stability of the DNA is generally measure by observing its melting temperature (T_m), which is defined as a temperature at which half of the double-helical DNA structure is unfolded to two individual strands.[45,46] In the present experiment, the value of T_m for ctDNA was determined by monitoring the absorbance of ctDNA in the presence and absence of 1f, 1h, 1i molecule by exciting the observable at 260 nm as a function of temperature ranging from 40 to 85 °C.[47,48] It is well-known that the intercalative binding of small molecules with the double helical DNA raise its T_m approximately an amount of 5–8 °C as compared to non bonded structure of ctDNA, whereas, the same for non-intercalative or groove binding structure of ctDNA is very less or sometimes no change in T_m is also found. The result of the present experiment is shown in Fig. 11 (a-c), where the normalized absorbance at 260 nm at various temperatures for bare ctDNA and 1f, 1h, 1i-ctDNA complex is presented black, red and green curve, respectively. The estimated value of T_m for bare ctDNA is 68.06, 67.92, 68.35 °C, while at the identical experimental conditions the same for 1f, 1h, 1i-ctDNA complex is 71.96, 69.62, 70.59^{0}C. A negligible difference between the estimated T_m value of bare ctDNA and 1f, 1h, 1i-ctDNA complex indicates a non-intercalative type of interaction in 1f, 1h, 1i-ctDNA complex. Slight increment in T_m for 1f, 1h, 1i-ctDNA complex as compared to bare ctDNA might be attributed for fact of altering conformation of ctDNA due to groove binding type of interaction between 1f, 1h, 1i and ctDNA.

3.3.8. Circular dichroism study

On the other hand, groove binding as well as electrostatic interactions of small molecule with ctDNA does not alter circular dichroism spectrum of ctDNA.[49] Fig. 12 (a-c) represents the circular dichroism spectrum of ctDNA, having a positive band at 275 nm due to stacking of base pair and a negative band at 245 nm due to characteristic helicity of the right-handed B-form. [50] These bands are entirely sensorial for binding interaction of small molecule with DNA.[51] This is conversant that stabilization or destabilization of ctDNA structure depends upon binding of a molecule with ctDNA. As shown in Fig. 10 (a-c), with increasing concentration of 1f, 1h, 1i there is negligible change in the circular dichroism spectra of ctDNA. These observations also discarded the chance of intercalation of 1f, 1h, 1i in the helical ctDNA and thereby suggest the minor groove binding of 1f, 1h, 1i with the host ctDNA molecule.

3.3.9. Molecular modelling and docking

Theoretical enumerations about the binding interaction of 1f, 1h, 1i and ctDNA can also be interpreted by performing the molecular modelling study. In this regards, the energy of the HOMO and LUMO plays a crucial role to find out the chemical stability (ΔE), chemical potential (μ), electrophilicity index (ω) and chemical hardness (η) of the molecules. [52] After optimizing the geometry, E_{HOMO} and E_{LUMO} was obtained and μ, η, ω and fraction number (ΔN) is calculated using following equations:

$$\mu = \frac{E_{LUMO} + E_{HOMO}}{2} \quad (7)$$

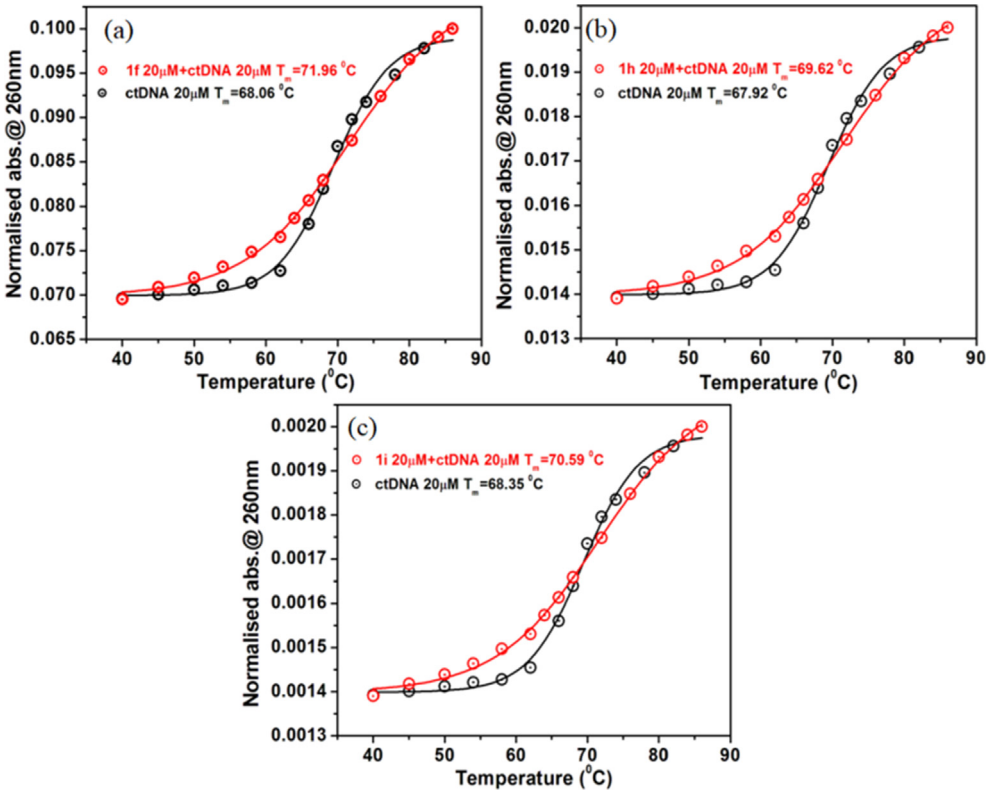

Fig. 11. (a-c) Thermal melting plot of free (black line) and complexed ctDNA (red line) with melting temperature in 0.01 M Tris-HCl buffer at pH 7.4. Maintains the fixed concentration of ctDNA (20 μM) and 1f, 1h, 1i was varied. The data represent mean ± 1% of three consecutive experiments.

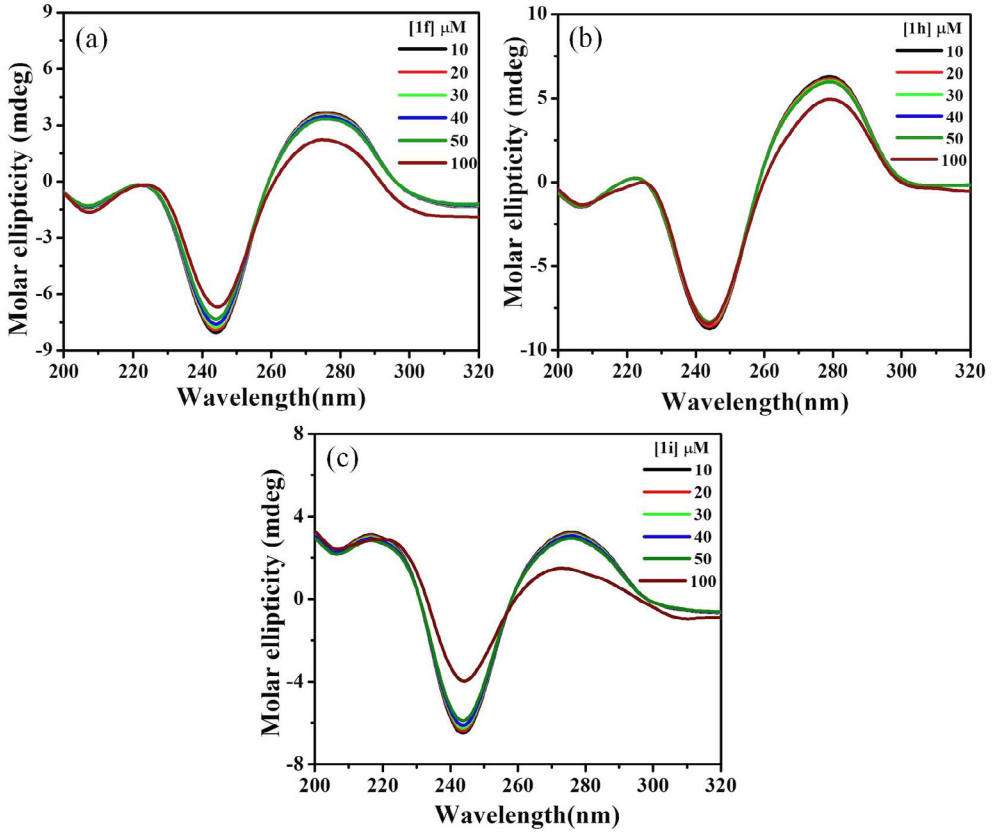

Fig. 12. (a-c) Circular dichroism spectra of ctDNA with increasing concentration of 1f, 1 h, 1i (0–100 μM) in 0.01 M Tris-HCl buffer at pH 7.4. Maintains the fixed concentration of ctDNA (20 μM) and 1f, 1h, 1i was varied. The data represent mean ± 1% of three consecutive experiments.

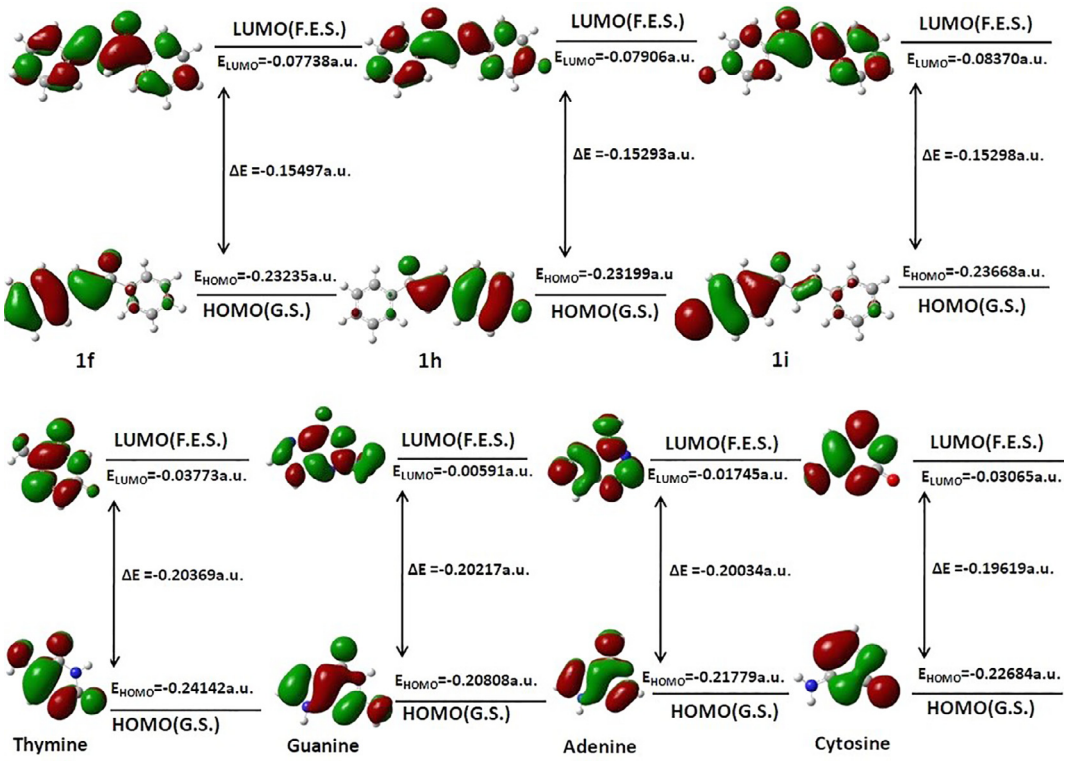

Fig. 13. Frontier molecular orbital's (gas phase), HOMO-LUMO composition of 1f, 1h, 1i and DNA bases. In figure G.S and F.E.S represents round state and first excited state.

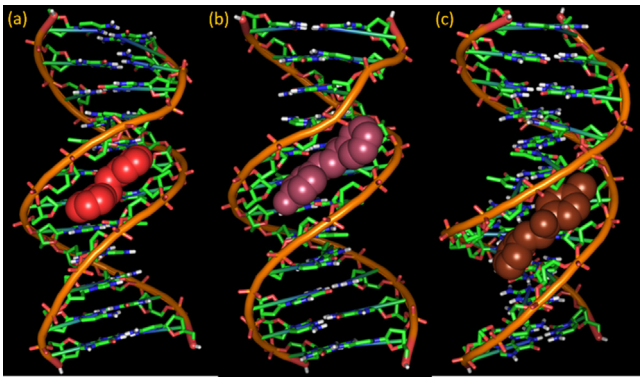

Fig. 14. Molecular docked representation of 1f,1h,1i-ctDNA complex (a), (b) and (c) showing minor groove binding of 1f, 1h, 1i with dodecamer duplex sequence d $(CGCGAATTCGCG)_2$ (PDBID: 1BNA). The relative free energy of binding the 1f, 1h, 1i-ctDNA complex system was found to be −8.86 kcal/ mol.

$$\eta = \frac{E_{LUMO} - E_{HOMO}}{2} \tag{8}$$

$$\omega = \mu^2/2\eta \tag{9}$$

$$\Delta N = \frac{\mu_A - \mu_B}{2(\eta_A + \eta_B)} \tag{10}$$

where μ_A, μ_B and η_A, η_B are the chemical potentials and chemical hardness of the system A (1f, 1h, 1i) and B (DNA bases), respectively. ΔN represents the fraction of number, which indicates electron transfer from system A to system B. The frontier molecular orbital diagrams of 1f, 1h, 1i and four DNA bases are presented in Fig. 13 with their energy values.

The values of charge transfer from A to B (following the values of ΔN) are presented in the Table S5. The calculated more negative value of μ of 1f, 1h, 1i as compared to DNA bases indicates higher electro-negativity of 1f,1h and 1i than DNA bases. This implies that during the binding interaction between 1f,1h,1i and ctDNA, electrons transfer occurs from DNA bases to 1f, 1h, 1i (cf. Table S5). As a result it is expected that 1f, 1 h, 1i can act as electron acceptor in following interaction with ctDNA. The molecular docking calculations of the present issue were performed in the quest of assign the mode of binding between the 1f, 1 h, 1i and ctDNA through disclosing the empirical binding spot. [24,35,53] It was carried out by the following mentioned protocol as documented in the experimental section. It is mentioned that the results of molecular docking analysis significantly depend on the chosen crystallographic ctDNA structure. We chose well-studied structure of B-DNA with PDB ID: 1BNA, to observe the exact position of the 1f, 1h, 1i in ctDNA helix. [49,50] The docked form is shown in Fig. 14, which demonstrates that 1f, 1h, 1i is found to be best fitted in the minor groove of double helix ctDNA with a free binding energy of −8.86 kcal/mol in good agreement with the same as found in a non-intercalative mode with ctDNA.[45,47]

The calculated free binding energy of 1f, 1h, 1i in ctDNA is also compared with the experimental free energy of binding and found that the molecular docking evaluated free energy of binding is consistent with the spectroscopic results as discussed above. Thus, the molecular docking analysis confirms the proposition of groove binding of 1f, 1h, 1i with ctDNA rather than the intercalative mode of binding.

4. Conclusion

In the present study, we have successfully explored potent anticancer activity of the compounds (1f, 1h, 1i) in particular against the PC3 cells and anti-microbial activity against model bacteria. All the synthetic compound interact non-covalently with the minor groove of the double helical ctDNA as evident from the UV–vis

absorbance, steady-state, time resolved fluorescence spectroscopy, thermal melting, denaturation, comparative displacement assays, ionic strength, circular dichroism along with the blind molecular docking study. A good agreement of the binding energy of the compounds in the minor groove of ctDNA is found between experimental and molecular docking study. *In vitro* cytotoxicity of the compounds were tested against human cancer cells PC3, A549, HCT116 and HeLa and normal NKE cell line by MTT assay. In this study, we found that all of the compounds significantly hindered the proliferation of various cancer cell lines in a dose-dependent manner and showed higher toxicity than that of normal kidney epithelial cell line, a prerequisite for developing any drug. Furthermore the compounds elicit higher cytotoxicity against the human prostate cancer cells (PC3) as compared to the other tested cancer cell lines. Apart from this the compounds exhibit appreciable antibacterial activity against model pathogenic bacteria with negligible hemolytic activity at their individual MICs. The apoptotic and cell cycle analysis demonstrate induced apoptosis in PC3 cancer cell by the compounds which was confirmed through FITC Annexin V/PI (flow cytometry) and DAPI staining assays. The compounds explicitly increased sub-G1 population in PC3 cell line and facilitate DNA damage mediated PC3 cell death. Henceforth, this study may serve as helpful complement for the exploration and progress of future medicinal and clinical applications of chalcone (1f) and its halo substituted analogue (1h,1i) as a prospective therapeutic agent.

Declaration of Competing Interest

The authors declare no conflict of interests.

Acknowledgement

AM, SG thanks UGC and CSIR for providing fellowship and BS wish to thanks DST-SERB for funding. AM wants to thank Prof. Pranab Sarkar for providing him to utilize the computational facility and Dr. Sudip Kr. Mondal, Department of Chemistry, Visva-Bharati, India for valuable discussion. Author thanks Dr. Kaushik Pal of Iowa State University, USA for helping us in CD experiments.

Appendix A. Supplementary data

Supplementary data to this article can be found online at https://doi.org/10.1016/j.molliq.2021.116504.

References

[1] (a) World Health Organization. Global Health Observatory. Geneva: World Health Organization; 2018. who.int/gho/database/en/.;
(b) R.L. Siegel, K.D. Miller, A. Jemal, Cancer Statistics, CA Cancer J. Clin. 68 (2018) 7–30;
(c) F. Bray, J. Ferlay, I. Soerjomataram, R.L. Siegel, L.A. Torre, A. Jemal, Global cancer statistics 2018: GLOBOCAN estimates of incidence and mortality worldwide for 36 cancers in 185 countries, CA Cancer J. Clin. 68 (2018) 394–424.

[2] N. Shankaraiah, K.P. Siraj, S. Nekkanti, V. Srinivasulu, P. Sharma, K.R. Senwar, M. Sathish, M.V.P.S. Vishnuvardhan, S. Ramakrishna, C. Jadala, N. Nagesh, A. Kamal, DNA-binding affinity and anticancer activity of β-carboline–chalcone conjugates as potential DNA intercalators: Molecular modelling and synthesis, Bioorg. Chem. 59 (2015) 130–139.

[3] R. Karki, P. Thapa, M.J. Kang, T.C. Jeong, J.M. Nam, H.-L. Kim, Y. Na, W.-J. Cho, Y. Kwon, E.-S. Lee, Synthesis, topoisomerase I and II inhibitory activity, cytotoxicity, and structure–activity relationship study of hydroxylated 2, 4-diphenyl-6-aryl pyridines, Bioorg. Med. Chem. 18 (2010) 3066–3077.

[4] M. F. A. Mohamed, M. Sh.A. Shaykoon, M. H. Abdelrahman, B. E. M. Elsadek, A. S. Aboraia, G. El-Din A. A. A. Rahma. Design, synthesis, docking studies and biological evaluation of novel chalcone derivatives as potential histone deacetylase inhibitors, Bioorg. Chem 72 (2017) 32-41.

[5] M.L. Go, X. Wu, X.L. Liu, Chalcones: an update on cytotoxic and chemoprotective properties, Curr. Med. Chem. 12 (2005) 481–499.

[6] H. Wei, J. Ruanb, X. Zhang, Coumarin–chalcone hybrids: promising agents with diverse pharmacological properties, RSC Adv. 6 (2016) 10846–10860.

[7] J.R. Dimmock, D.W. Elias, M.A. Beazely, N.M. Kandepu, Bioactivities of chalcones, Curr. Med. Chem. 6 (1999) 1125–1149.

[8] (a) B. Havsteen, Flavonoids, a class of natural products of high pharmacological potency, Biochem. Pharmacol. 32 (1983) 1141–1148;
(b) J.B. Harborne, H. Baxter, The handbook of natural flavonoids Vols 1 (1999) 2;
(c) M. Elliott, K. Chithan, The impact of plant flavonoids on mammalian biology: implications for immunity, inflammation and cancer, in: J.B. Harborne (Ed.), The flavonoids: advances in research since 1986, Chapman and Hall, London, UK, 1993;
(d) T.P.T. Cushnie, A.J. Lamb, Antimicrobial activity of flavonoids, Int. J. Antimicrob. 26 (2005) 343–356;
(e) J.B. Harborne, C.A. Williams, Advances in flavonoid research since 1992, Phytochemistry 55 (2000) 481–504;
(f) C.F. Skibola, M.T. Smith, Potential health impacts of excessive flavonoid intake, Free Radic Biol Med 29 (2000) 375–383;
(g) E. Middleton, C. Kandaswami, T.C. Theoharides, The Effects of Plant Flavonoids on Mammalian Cells: Implications for Inflammation, Heart Disease, and Cancer, Pharmacol Rev 52 (2000) 673–751;
(h) P. Singh, A. Anand, V. Kumar, Recent developments in biological activities of chalcones: a mini review, Eur. J. Med. Chem. 85 (2014) 758–777.

[9] M.A. Husain, H.M. Ishqi, S.U. Rehman, T. Sarwar, S. Afrin, Y. Rahman, M. Tabish, Elucidating the interaction of sulindac with calf thymus DNA: biophysical and in silico molecular modelling approach, New J. Chem. 41 (2017) 14924–14935.

[10] N. Ranjan, P. Kellish, A. King, D.P. Arya, Impact of linker length and composition on fragment binding and cell permeation: Story of a bisbenzimidazole dye fragment, Biochemistry 56 (2017) 6434–6447.

[11] S.E. Osborne, A.D. Ellington, Nucleic acid selection and the challenge of combinatorial chemistry, Chem. Rev. 97 (1997) 349–370.

[12] M.M. Becker, P.B. Dervan, Molecular recognition of nucleic acid by small molecules. Binding affinity and structural specificity of bis (methidium) spermine, J. Am. Chem. Soc. 101 (1979) 3664–3666.

[13] A.A. Almaqwashi, T. Paramanathan, I. Rouzina, M.C. Williams, Mechanisms of small molecule–DNA interactions probed by single-molecule force spectroscopy, Nucleic Acids Res. 44 (2016) 3971–3988.

[14] A. Mukherjee, S. Ghosh, R. Sarkar, S. Samanta, S. Ghosh, M. Pal, A. Majee, S.K. Sen, B. Singh, Synthesis, characterization and unravelling the molecular interaction of new bioactive 4-hydroxycoumarin derivative with biopolymer: Insights from spectroscopic and theoretical aspect, J. Photochem. Photobiol., B 189 (2018) 124–137.

[15] H. Morinaga, T. Bando, T. Takagaki, M. Yamamoto, K. Hashiya, H. Sugiyama, Cysteine cyclic pyrrole–imidazole polyamide for sequence-specific recognition in the DNA minor groove, J. Am. Chem. Soc. 183 (2011) 18924–18930.

[16] D.P. Arya, B. Willis, Reaching into the Major Groove of B-DNA: Synthesis and Nucleic Acid Binding of a Neomycin-Hoechst 33258 Conjugate, J. Am. Chem. Soc. 125 (2003) 12398–12399.

[17] K. Schäfer, H. Ihmels, E. Porcù, G. Viola, Control of the DNA-Binding and Antiproliferative Properties of Hydroxybenzo[b]quinolizinium Derivatives with pH and Light, Chem. Eur. J. 23 (2017) 370–379.

[18] P.M. Reddy, T.C. Bruice, Solid-Phase Synthesis of Positively Charged Deoxynucleic Guanidine (DNG) Tethering a Hoechst 33258 Analogue: Triplex and Duplex Stabilization by Simultaneous Minor Groove Binding, J. Am. Chem. Soc. 126 (2004) 3736–3747.

[19] M.S. Blackledge, C. Melander, Programmable DNA-binding small molecules, Bioorg. & Med. Chem. 21 (2013) 6101–6114.

[20] D.E. Wemmer, Ligands recognizing the minor groove of DNA: development and applications, Biopolymers 52 (1999) 197–211.

[21] I. Yousuf, F. Arjmand, S. Tabassum, L. Toupet, R.A. Khan, M.A. Siddiqui, Mechanistic insights into a novel chromone-appended Cu (II) anticancer drug entity: in vitro binding profile with DNA/RNA substrates and cytotoxic activity against MCF-7 and HepG2 cancer cells, Dalton Trans. 44 (2015) 10330–10342.

[22] M. J. Frisch, G. W. Trucks, H. B. Schlegel, G. E. Scuseria, M. A. Robb, J. R. Cheeseman, G. Scalmani, V. Barone, B. Mennucci, G. A. Petersson. et al. Gaussian 09, revision B.01; Gaussian, Inc.: Wallingford, CT, 2010.

[23] (a) P. Li, Y. Bu, H. Ai, Density Functional Studies on Conformational Behaviors of Glycinamide in Solution, J. Phys. Chem. B 108 (2004) 1405–1413;
(b) H.-Y. Li, M. Pu, K.H. Liu, B.F. Zhang, B.-H. Chen, A density-functional theory study on double-bond isomerization of 1-butene to cis-2-butene catalyzed by zeolites, Chem. Phys. Lett. 404 (2005) 384–388;
(c) L.L.G. Justino, M.L. Ramos, P.E. Abreu, R.A. Carvalho, A.J.F.N. Sobral, U. Scherf, H.D. Burrows, Conformational Studies of Poly(9,9-dialkylfluorene)s in Solution Using NMR Spectroscopy and Density Functional Theory Calculations, J. Phys. Chem. B 113 (2009) 11808–11821;
(d) M. Haghdadi, N. Farokhi, Density functional theory (DFT) calculations of conformational energies and inter conversion pathways in 1, 2, 7-thiadiazepane, J. Serb. Chem. Soc. 76 (2011) 395–406;
(e) M. Szczepaniak, J. Moc, Conformational studies of gas-phase ribose and 2-deoxyribose by density functional, second order PT and multi-level method calculations: the pyranoses, furanoses, and open-chain structures, Carbohydr. Res. 384 (2014) 20–36.

[24] A. Mukherjee, B. Singh, Binding interaction of pharmaceutical drug captopril with calf thymus DNA: a multispectroscopic and molecular docking study, J. Lumin. 190 (2017) 319–327.

[25] J.R. Lakowicz, Principles of Fluorescence Spectroscopy, 3rd ed., Springer, New York, 2006.

[26] A. Mukherjee, T. Chaudhuri, S.P. Moulik, M. Banerjee, Internal charge transfer based ratiometric interaction of anionic surfactant with calf thymus DNA bound cationic surfactant: Study I, Spectrochim. Acta Part A Mol. Biomol. Spectrosc. 152 (2016) 1–7.
[27] A. Mukherjee, S. Mondal, B. Singh, Spectroscopic, electrochemical and molecular docking study of the binding interaction of a small molecule 5H-naptho[2,1-f][1,2] oxathieaphine 2,2-dioxide with calf thymus DNA, Int. J. Biol. Macromol. 101 (2017) 527–535.
[28] M.H. Grant, K.C. Wu, W.R. Bauer, S.J. Lippard, Binding of platinum and palladium metallo intercalation reagents and antitumor drugs to closed and open DNAs, Biochemistry 15 (1976) 4339–4346.
[29] G. M. Morris, D. S. Goodsell, R. S. Halliday, R. Huey, W. E. Hart, R. K. Belew, A. J. Olson Automated docking using a Lamarckian genetic algorithm and an empirical binding free energy function, J. Comput. Chem.19 (1998) 1639-1662.
[30] W.L. De Lano, The PyMOL Molecular Graphics System, De Lano Scientific, San Carlos, CA, 2004.
[31] W.P. Roos, B. Kaina, DNA damage-induced cell death by apoptosis, Trends Mol. Med. 12 (2006) 440–450.
[32] E.P. Rogakou, D.R. Pilch, A.H. Orr, V.S. Ivanova, W.M. Bonner, DNA double-stranded breaks induce histone H2AX phosphorylation on serine 139, The Journal of biological chemistry 273 (1998) 5858–5868.
[33] A. Mukherjee, S. Ghosh, M. Pal, B. Singh, Deciphering the effective sequestration of DNA bounded bioactive small molecule Safranin-O by non-ionic surfactant TX-114 and diminution its cytotoxicity, J. Mol. Liq. 289 (2019) 111116.
[34] (a) B. Rafique, A.M. Khalid, K. Akhtar, A. Jabbar, Interaction of anticancer drug methotrexate with DNA analyzed by electrochemical and spectroscopic methods, Biosens. Bioelectron. 44 (2013) 21–26;
(b) P.D. Ross, S. Subramanian, Thermodynamics of Protein Association Reactions: Forces Contributing to Stability, Biochemistry 20 (1981) 3096–3102;
(c) F. Leng, J.B. Chaires, M.J. Waring, Nucleic Acids Res. 31 (2003) 6191–6197.
[35] F.A. Qais, K.M. Abdullah, Md.M. Alam, I. Naseem, I. Ahmad, Interaction of capsaicin with calf thymus DNA: A multi-spectroscopic and molecular modelling study, Int. J. Biol. Macromol. 97 (2017) 392–402.
[36] H.K. Liu, P.J. Sadler, Interaction of capsaicin with calf thymus DNA: A multi-spectroscopic and molecular modelling study, Acc. Chem. Res. 44 (2011) 349–359.
[37] S.U. Rehman, Z. Yaseen, M.A. Husain, T. Sarwar, H.M. Ishqi, M. Tabish, Interaction of 6 Mercaptopurine with Calf Thymus DNA–Deciphering the Binding Mode and Photoinduced DNA Damage, PLoS ONE 9 (2014) e93913.
[38] M.B. Lyles, I.L. Cameron, Interactions of the DNA intercalator acridine orange, with itself, with caffeine, and with double stranded DNA, Biophys. Chem. 96 (2002) 53–76.
[39] R. Kakkar, R. Garg, Suruchi, Theoretical study of tautomeric structures and fluorescence spectra of Hoechst 33258, THEOCHEM 579 (2002) 109–113.
[40] Y.M. Song, J.W. Kang, J. Zhou, Z.H. Wang, X.Q. Lu, L.F. Wang, J.Z. Gao, Study on the fluorescence spectra and electrochemical behavior of ZnL_2 and Morin with DNA, Spectrochim. Acta Part A Mol. Biomol. Spectrosc. 56 (2000) 2491–2497.
[41] J. Olmsted, D.R. Kearns, Mechanism of ethidium bromide fluorescence enhancement on binding to nucleic acids, Biochemistry 16 (1977) 3647–3654.
[42] Y. Guan, W. Zhou, X. Yao, M. Zhao, Y. Li, Determination of nucleic acids based on the fluorescence quenching of Hoechst 33258 at pH 4.5, Anal. Chim. Acta 570 (2006) 21–28.
[43] X. Zhou, G. Zhang, L. Wang, Probing the binding mode of psoralen to calf thymus DNA Int, J. Biol. Macromol. 67 (2014) 228–237.
[44] C.V. Kumar, R.S. Turner, E.H. Asuncion, Groove binding of a styrylcyanine dye to the DNA double helix: the salt effect, J. Photochem. Photobiol., A 74 (1993) 231–238.
[45] E.V. Hackl, Y.P. Blagoi, Urea effect on Cu^{2+}-induced DNA structural transitions in solution, J. Inorg. Biochem. 98 (2004) 1911–1920.
[46] F.Y. Wu, F.Y. Xie, Y.M. Wu, J.I. Hong, Interaction of a New Fluorescent Probe with DNA and its Use in Determination of DNA, J. Fluoresc. 18 (2008) 175–181.
[47] S.S. Wijeratne, J.M. Patel, C.H. Kiang, Melting Transitions of DNA-Capped Gold Nanoparticle Assemblies, Rev. Plasmonics. 2012 (2010) 269–282.
[48] J. L. Mergny, G. D-Valentin, C. H. Nguyen, L. Perrouault, B. Faucon, M. Rougee, T. M.-Garestier, E. Bisagni, C. Ĥel'ene, Triple helix-specific ligands, Science 256 (1992) 1681-1684.
[49] K. Holde, W.C. Johnson, P.S. Ho, Principles of physical biochemistry, Prentice-Hall, New York, 1998.
[50] T. Sarwar, S.U. Rehman, M.A. Husain, H.M. Ishqi, M. Tabish, Interaction of coumarin with calf thymus DNA: deciphering the mode of binding by in vitro studies, Int. J. Biol. Macromol. 73 (2015) 9–16.
[51] B.K. Paul, N. Guchhait, Exploring the Strength, Mode, Dynamics, and Kinetics of Binding Interaction of a Cationic Biological Photosensitizer with DNA: Implication on Dissociation of the Drug–DNA Complex via Detergent Sequestration, J. Phys. Chem. B 115 (2011) 11938–11949.
[52] J. Padmanabhan, R. Parthasarathi, V. Subramanian, P.K. Chattaraj, Group philicity and electrophilicity as possible descriptors for modeling ecotoxicity applied to chlorophenols, Chem. Res. Toxicol. 19 (2006) 356–364.
[53] K. Zheng, F. Liu, X.M. Xu, Y.T. Li, Z.Y. Wua, C.-W. Yan, Synthesis, structure and molecular docking studies of dicopper (ii) complexes bridged by N-phenolato-N′-[2-(dimethylamino)ethyl] oxamide: the influence of terminal ligands on cytotoxicity and reactivity towards DNA and protein BSA, New J. Chem. 38 (2014) 2964–2978.